Journal Pre-proof

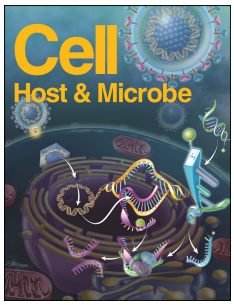

Induction of alarmin S100A8/A9 mediates activation of aberrant neutrophils in the pathogenesis of COVID-19

Qirui Guo, Yingchi Zhao, Junhong Li, Jiangning Liu, Xiuhong Yang, Xuefei Guo, Ming Kuang, Huawei Xia, Zeming Zhang, Lili Cao, Yujie Luo, Linlin Bao, Xiao Wang, Xuemei Wei, Wei Deng, Nan Wang, Luoying Chen, Jingxuan Chen, Hua Zhu, Ran Gao, Chuan Qin, Xiangxi Wang, Fuping You

PII: S1931-3128(20)30679-X

DOI: https://doi.org/10.1016/j.chom.2020.12.016

Reference: CHOM 2443

To appear in: *Cell Host and Microbe*

Received Date: 29 August 2020

Revised Date: 11 November 2020

Accepted Date: 21 December 2020

Please cite this article as: Guo, Q., Zhao, Y., Li, J., Liu, J., Yang, X., Guo, X., Kuang, M., Xia, H., Zhang, Z., Cao, L., Luo, Y., Bao, L., Wang, X., Wei, X., Deng, W., Wang, N., Chen, L., Chen, J., Zhu, H., Gao, R., Qin, C., Wang, X., You, F., Induction of alarmin S100A8/A9 mediates activation of aberrant neutrophils in the pathogenesis of COVID-19, *Cell Host and Microbe* (2021), doi: https://doi.org/10.1016/j.chom.2020.12.016.

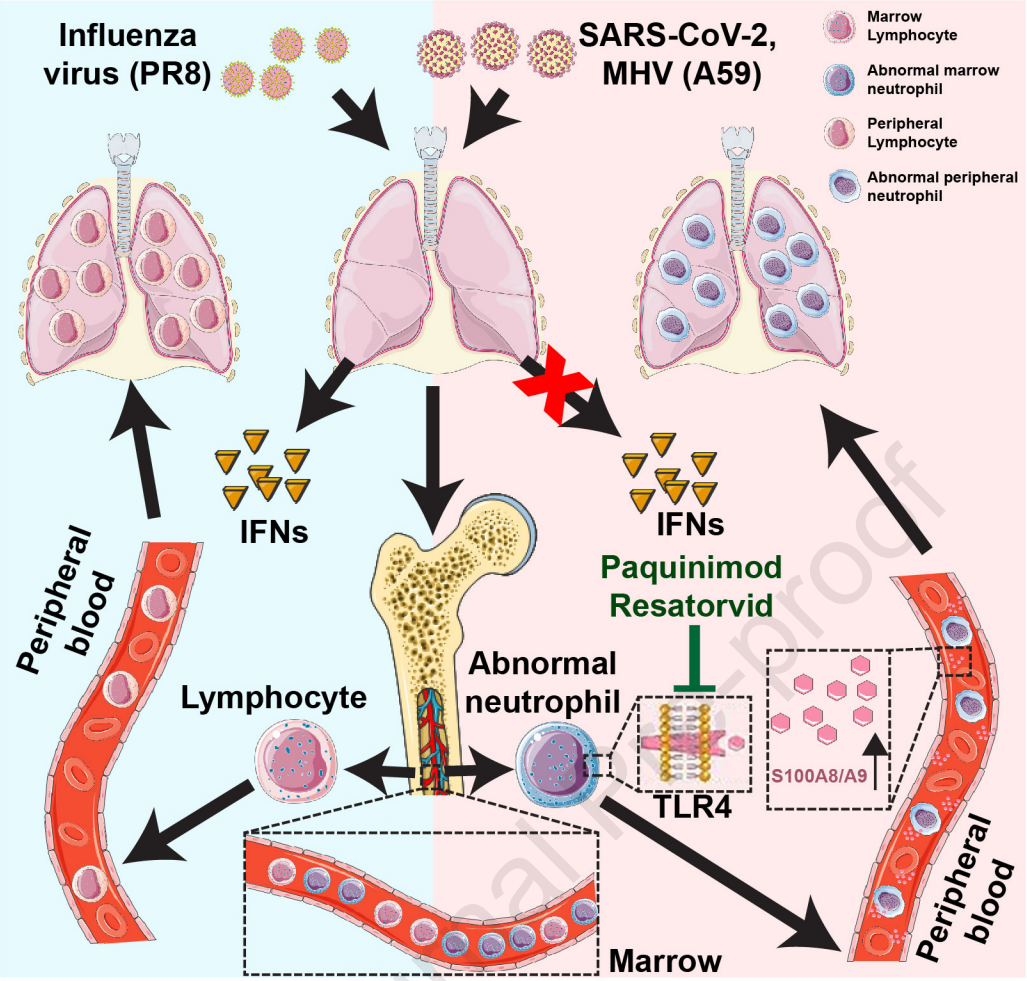

Induction of alarmin S100A8/A9 mediates activation of aberrant neutrophils in the pathogenesis of COVID-19

Qirui Guo[1,4], Yingchi Zhao[1,4], Junhong Li[2,4], Jiangning Liu[3,4], Xiuhong Yang[3,4], Xuefei Guo[1], Ming Kuang[1], Huawei Xia[1], Zeming Zhang[1], Lili Cao[1], Yujie Luo[1], Linlin Bao[3], Xiao Wang[1], Xuemei Wei[1], Wei Deng[3], Nan Wang[2], Luoying Chen[1], Jingxuan Chen[1], Hua Zhu[3], Ran Gao[3], Chuan Qin[3]*, Xiangxi Wang[2]*, Fuping You[1,5]*

[1]Institute of Systems Biomedicine, Department of Immunology, School of Basic Medical Sciences, Beijing Key Laboratory of Tumor Systems Biology, Peking University Health Science Center, Beijing, China.

[2]University of Chinese Academy of Sciences, CAS Key Laboratory of Infection and Immunity, National Laboratory of Macromolecules, Institute of Biophysics, Chinese Academy of Sciences, Beijing, China.

[3]Key Laboratory of Human Disease Comparative Medicine, Chinese Ministry of Health, Beijing Key Laboratory for Animal Models of Emerging and Remerging Infectious Diseases, Institute of Laboratory Animal Science, Chinese Academy of Medical Sciences and Comparative Medicine Center, Peking Union Medical College, Beijing, China.

[4]These authors contributed equally to this work.

[5]Lead Contact.

*Correspondence: qinchuan@pumc.edu.cn (C.Q.), xiangxi@ibp.ac.cn (X.-X.W.), fupingyou@hsc.pku.edu.cn (F.-P.Y.).

Summary

The SARS-CoV-2 pandemic poses an unprecedented public health crisis. Evidence suggests that SARS-CoV-2 infection causes dysregulation of the immune system. However, the unique signature of early immune responses remains elusive. We characterized the transcriptome of rhesus macaques and mice infected with SARS-CoV-2. Alarmin S100A8 was robustly induced in SARS-CoV-2 infected animal models as well as in COVID-19 patients. Paquinimod, a specific inhibitor of S100A8/A9, could rescue the pneumonia with substantial reduction of viral loads in SARS-CoV-2 infected mice. Remarkably, Paquinimod treatment resulted in almost 100% survival in a lethal model of mouse coronavirus infection using the mouse hepatitis virus (MHV). A group of neutrophils that contributes to the uncontrolled pathological damage and onset of COVID-19 were dramatically induced by coronavirus infection. Paquinimod treatment could reduce these neutrophils and regain antiviral responses, unveiling key roles of S100A8/A9 and aberrant neutrophils in the pathogenesis of COVID-19, highlighting new opportunities for therapeutic intervention.

Keywords

SARS-CoV-2, S100A8/A9, aberrant neutrophils, Paquinimod

Introduction

The ongoing Coronavirus Disease 2019 (COVID-19) caused by severe acute respiratory syndrome coronavirus-2 (SARS-CoV-2) has resulted in unprecedented public health crises, requiring a deep understanding of the pathogenesis and developments of effective COVID-19 therapeutics (Wu et al., 2020b; Zhu et al., 2020). Innate immunity is an important arm of the mammalian immune system, which serves as the first line of host defense against pathogens. Most of the cells of the body harbor the protective machinery of the innate immunity and can recognize foreign invading viruses (Akira et al., 2006). The innate immune system recognizes microorganisms via the pattern-recognition receptors (PRRs) and upon detection of invasion by pathogens, PRRs activate downstream signaling pathways leading to the expression of various cytokines and immune-related genes for clearing the pathogens including bacteria, viruses and others (Akira et al., 2006). With regards to SARS-CoV-2 infection, an overaggressive immune response has been noted which causes immunopathology (Huang et al., 2020; Zhang et al., 2020). In addition, T cell exhaustion or dysfunction has also been observed (Diao et al., 2020; Zheng et al., 2020a; Zheng et al., 2020b). Additional studies suggest that there may be a unique immune response evoked by coronaviruses (Blanco-Melo et al., 2020). However, the nature of these responses elicited by the virus remains poorly understood.

Accumulating evidences suggest that the neutrophil count is significantly increased in COVID-19 patients with severe symptoms (Kuri-Cervantes et al., 2020; Liao et al., 2020; Tan et al., 2020; Wu et al., 2020a). It is believed that neutrophils migrate from the circulating blood to infected tissues in response to inflammatory stimuli, where they protect the host by phagocytizing, killing and digesting bacterial and fungal pathogens (Nauseef and Borregaard, 2014; Nicolas-Avila et al., 2017). The role of such a response in host defense against viral infection has not been clearly characterized. A recent study observed a new subpopulation of neutrophils in COVID-19 patients, which have been named developing neutrophils because they lack canonical neutrophil markers like

CXCR2 and FCGR3B (Wilk et al., 2020). However, it is still not clear how this type of neutrophil is induced. Moreover, the precise function of these cells is also unknown.

Alarmins are endogenous, chemotactic and immune activating proteins/peptides that are released as a result of cell injury or death, degranulation, or in response to infection. They relay intercellular defense signals by interacting with pattern-recognition receptors (PRRs) to activate immune cells in host defense (Oppenheim and Yang, 2005; Yang et al., 2017). Currently, the major categories of alarmins include defensins, high-mobility group (HMG) proteins, interleukins (ILs), heat shock proteins (HSPs), S100 proteins, uric acid, hepatoma derived growth factor (HDGF), eosinophil-derived neurotoxin (EDN), and cathelin-related antimicrobial peptide (CRAMP) (Giri et al., 2016; Yang et al., 2017). In response to microbial infection, alarmins are released to initiate and amplify innate/inflammatory immune responses, which involve the activation of resident leukocytes (e.g. macrophages, dendritic cells, mast cells, etc.), production of inflammatory mediators (cytokines, chemokine and lipid metabolites), recruitment of neutrophils and monocytes/macrophages for the purpose of eliminating invading microorganisms and clearing injured tissues (Bianchi, 2007; Chen and Nunez, 2010; Nathan, 2002; Oppenheim and Yang, 2005; Yang et al., 2017). However, uncontrolled production of alarmins is harmful or even fatal to the host in some cases. HMGB1 protein acts as a late mediator of lethal systemic inflammation in sepsis (Wang et al., 2004). Therefore, anti-HMGB1 therapeutics have shown to be beneficial in experimental models of sepsis.

S100A8 and S100A9, members of the S100 group of proteins, make up approximately 45% of the cytoplasmic proteins present in neutrophils. They are also referred to as MRP8 and MRP14, respectively. Under physiological conditions, massive levels of S100A8 and S100A9 are stored in neutrophils and myeloid-derived dendritic cells, while low levels of S100A8 and S100A9 are expressed constitutively in monocytes (Foell et al., 2004; Wang et al., 2018). S100A8 and S100A9 often form heterodimers (S100A8/A9) (Ometto et al., 2017). The major functions of S100A8/A9

reported so far include the regulation of leukocyte migration and trafficking, the remodeling of cytoskeleton and amplification of inflammation and exertion of anti-microbial activity (Ometto et al., 2017; Wang et al., 2018). After being infected with bacteria, neutrophils, macrophages and monocytes intensely induce the expression and secretion of S100A8/A9 to modulate inflammatory processes through the induction of inflammatory cytokines. S100A8/A9 is an endogenous ligand of toll-like receptor 4 (TLR4), and can trigger multiple inflammatory pathways mediated by TLR4 (Vogl et al., 2007). The receptor for advanced glycation end products (RAGE) pathways can also be activated by S100A8/A9 (Narumi et al., 2015). S100A8 and S100A9 also have antibacterial potential via their ability to bind Zn^{2+} (Foell et al., 2004; Wang et al., 2018). However, not much is known about the roles of S100A8/A9 in host defense responses against viruses.

In the present study, we characterized the nature of the early innate immune responses evoked in rhesus macaques and mice during SARS-CoV-2 infection. S100A8 was dramatically up-regulated by SARS-CoV-2 and a mouse coronavirus (mouse hepatitis virus, MHV), but not by other viruses. A group of non-canonical aberrant neutrophils were activated during SARS-CoV-2 infection. The abnormal immune responses were mediated by the S100A8/A9-TLR4 pathway. S100A8/A9 specific inhibitor, Paquinimod, significantly reduced the number of aberrant neutrophils induced by the coronavirus, inhibited viral replication and rescued lung damage. These results highlight the potential of therapeutically targeting S100A8/A9 for suppressing the uncontrolled immune response associated with severe cases of COVID-19 and provide information on alarmin-mediated pathway for regulating neutrophils.

Results

SARS-CoV-2 infection induces alarmin *S100A8* expression and neutrophils chemotaxis

To characterize the early immune responses against SARS-CoV-2 infection, we

infected rhesus macaques with SARS-CoV-2 and analyzed the transcriptome of lung and blood at day 0, day 3 and day 5 post infection (5 dpi) (Figure 1A and S1A). Gene Ontology (GO) analysis showed that a small group of genes involved in defense responses against viruses were induced in the infected lungs (Figure 1B), and type I IFNs was not induced by SARS-CoV-2 infection (Figure S1B). However, interestingly, a greater number of genes involved in regulating cellular responses to lipopolysaccharide (LPS) and neutrophil chemotaxis were induced (Figure 1B). Kyoto Encyclopedia of Genes and Genomes（KEGG) pathways analysis also showed that SARS-CoV-2 induced genes were enriched in anti-bacterial pathways (Figure S1C). Meanwhile, combined with the elevated neutrophils in COVID-19 patients with severe symptoms (Kuri-Cervantes et al., 2020; Liao et al., 2020; Tan et al., 2020; Wu et al., 2020a), we hypothesized that neutrophils, which play an important anti-bacterial function, may be abnormally activated at the very beginning of SARS-CoV-2 infection. Thus, we analyzed the expression of neutrophil markers in the lungs from rhesus macaques at day 0, day 3 and day 5 post infection. The results showed that all the neutrophil marker genes were significantly induced as a result of SARS-CoV-2 infection (Figure 1C). Markers for monocytes and natural killer cells were slightly up-regulated, and T cells were unchanged, while B cells were significantly down-regulated in the lungs of rhesus macaques infected by SARS-CoV-2 (Figure S1D and S1E). These suggested that the SARS-CoV-2 infection provoked a non-canonical antiviral response or an anti-bacterial response accompanied by increased neutrophils in the lung at the early stage.

To explore how SARS-CoV-2 infection triggered the activation of anti-bacterial responses, the differential expression of genes before and after SARS-CoV-2 infection were examined. The results showed that the expression of *S100A8* was robustly up-regulated at 3 dpi and 5 dpi after SARS-CoV-2 infection (Figure 1D). S100A8 acts as an alarmin through formation of heterodimers with S100A9, and then functions as danger associated molecular pattern (DAMP) molecules and activates innate immune

responses via binding to pattern recognition receptors (PRR), such as Toll-like receptor 4 (TLR4) (Chakraborty et al., 2017). Further, we found that S100A8 was the most significantly induced gene among all the known alarmins (Figure 1E). Subsequently, through qRT-PCR analysis, we verified that the level of *S100A8* surged along with an increase in the viral loads in the lungs of rhesus macaques infected by SARS-CoV-2 (Figure 1F). Next, we examined the expression of alarmins and neutrophil marker genes in the blood samples from infected rhesus macaques. *S100A8/A9* and the neutrophil marker genes were also induced in the blood by the SARS-CoV-2 infection (Figure 1G). We further investigated if *S100A8* were up-regulated in COVID-19 patients. Analysis of alarmins by RNA-seq data showed that both *S100A8* and neutrophil marker genes were up-regulated in post-mortem lung samples from COVID-19 patients, compared with biopsied healthy lung tissue from uninfected individuals (Figure 1H). Concomitantly, the mRNA level of S100A8 in peripheral blood from COVID-19-positive patients was significantly higher when compared to healthy subjects (Figure S1F). A group of alarmins were induced in different types of blood cells of COVID-19-positive patients, in which S100A8 was prominently induced in $CD14^{+}$ monocytes, neutrophils and developing neutrophils (Figure S1G). S100A8/A9 can act as the ligand of TLR4, which is the primary PRR that recognizes invading gram-negative bacterium. Therefore, elevated *S100A8* expression may be responsible for the activation of anti-bacterial pathways and neutrophil chemotaxis. Above all, S100A8 probably play an important role in the course of SARS-CoV-2 infection.

Aberrant induction of *S100A8* is triggered by coronaviruses but not by other viruses

To further study the relationship between S100a8 expression and neutrophils chemotaxis and SARS-CoV-2 infection, we challenged human *ACE2* (*hACE2*) transgenic mice with SARS-CoV-2 and performed RNA-seq analysis of lungs to

characterize the defense responses during viral infection (Figure 2A and S2A). Consistent with the results from the rhesus macaque, genes induced by SARS-CoV-2 infection in mice were also enriched in anti-bacterial humoral response and neutrophil chemotaxis, and did not trigger typical antiviral immune responses (Figure 2B and S2B). Meanwhile, *S100a8* and the neutrophil marker genes (*Ly6g, Mmp8,* etc.) were robustly up-regulated at 5 dpi when the mice developed sicker (Figure 2C and 2D). Consistent results across different species suggested that the sharp up-regulation of *S100a8* and neutrophils chemotaxis is closely related to the formation of fatal infections by SARS-CoV-2 infection.

We then constructed a mouse model of canonical pneumonia with influenza A virus (IAV) (Figure S2C). RNA-seq analysis of lungs showed that, compared with SARS-CoV-2 infection, IAV infection induced genes were enriched in defense response to virus and cellular response to IFNβ (Figure 2B and S2B). We further analyzed the differentially induced genes by SARS-CoV-2 and IAV at different time intervals after infection. The results showed that IAV induced canonical antiviral responses and activated type I IFNs signaling, while the expression of the classical antiviral molecules *Ifnb1* and *Isg15* was severely impaired and the anti-bacterial responses, neutrophil related processes were induced during SARS-CoV-2 infection (Figure 2C, S2D and S2E). However, IAV infection did not induced *S100a8* and neutrophil marker genes expression (Figure 2C, 2D and S2F). These suggested that the intense expression of *S100a8* and neutrophils chemotaxis was specifically present during SARS-CoV-2 infection.

To further confirm this, we infected C57BL/6 mice with other RNA- or DNA-viruses including encephalomyocarditis virus (EMCV) and herpes simplex virus 1 (HSV-1), and measured the expression of S100A8 in the blood and lungs of infected animals. Neither of these viruses were able to induce the expression of *S100a8* (Figure 2E). We investigated if other coronaviruses were able to induce the transcription of *S100a8* and neutrophils chemotaxis. We first infected C57BL/6 mice

with mouse hepatitis virus (MHV-A59) intranasally. However, no obvious symptoms in infected mice were observed. Further, we infected IRF3/IRF7 double knockout mice and IFNAR deficient mice with MHV. Similar to the wild type C57BL/6 mice, IRF3/IRF7 double knockout mice were able to eliminate the virus rapidly and did not develop severe pneumonia. Interestingly, we found that all the IFNAR deficient mice infected with MHV suddenly became sicker and died with a sharp increase in *S100a8* and *Ly6g* at 3-7 dpi, and the lungs of infected mice showed obvious lesions (Figure 2F and S3A). Meanwhile, RNA-seq analysis of the lungs showed that the genes induced by MHV were also enriched in neutrophil chemotaxis and anti-bacterial pathways (Figure 2G). Compared with IAV infection, type I IFNs induction was impaired and neutrophil marker genes were significantly induced in MHV infection (Figure 2H, S2E, S3B and S3C). Taken together, SARS-CoV-2 and MHV, both coronaviruses, induced an almost uniform immune response. Thus, *S100a8* expression and neutrophil chemotaxis is likely a specific feature of coronavirus infection, and involved in the formation of fatal coronavirus infections.

Coronavirus infection induces the invasion of aberrant neutrophils

The activation of anti-bacterial pathway, neutrophil chemotaxis and high expression of *S100a8* all indicated the abnormality of neutrophils in coronavirus infection including SARS-CoV-2 and MHV. Therefore, we examined neutrophils infiltration in the lungs of infected mice. As the main cytoplasmic protein of neutrophils, S100A8 can accurately indicate neutrophils in lung tissue. Thus, immunohistochemical staining for S100A8 of the lungs in SARS-CoV-2 infection and MHV infection at 5 dpi was performed. The results showed that, compared with the control group, neutrophils ($S100A8^{+}$) invading the lungs were significantly increased in both SARS-CoV-2 and MHV infection (Figure 3A). This suggested that coronavirus infection does induce the invasion of neutrophils.

To further accurately define neutrophil invasion during SARS-CoV-2 and MHV infection, the neutrophils in the lungs of infected mice were analyzed by flow

cytometry (Figure S4A). The results showed that almost all the neutrophils in the control group were typical $CD45^{+}CD11b^{+}Ly6G^{high}$. Surprisingly, however, most neutrophils in SARS-CoV-2- and MHV-infected mice showed $CD45^{+}CD11b^{+}Ly6G^{variable}$ (Figure 3B). This indicated that neutrophils in coronavirus infected mice were distorted. To investigate whether other viruses or stimuli are able to induce the production of this particular group of neutrophils, we challenged mice with IAV, EMCV, HSV and LPS. The results showed that although these infections caused fluctuations in the number of neutrophils, these neutrophils were still $CD45^{+}CD11b^{+}Ly6G^{high}$ and did not appear abnormal (Figure 3C). These suggested that coronavirus infection induced the invasion of a group of aberrant neutrophils.

To investigate the source of this population of aberrant neutrophils, we analyzed the peripheral blood and bone marrow of coronavirus infected mice by flow cytometry. Shockingly, neutrophils are also aberrant in the peripheral blood of SARS-CoV-2- and MHV-infected mice, even in the bone marrow (Figure S4B and 3D). The relatively low Ly-6G levels in aberrant neutrophils suggested that it may be an immature cell. Further, we purified the aberrant neutrophils in bone marrow of MHV-infected mice by flow cytometry sorting, and analyzed the expression of marker gene (*Cxcr2* and *Fcgr3*) of mature neutrophils in these aberrant neutrophils. The qRT-PCR results showed that, compared with the normal neutrophils in control group, the expression of *Cxcr2* and *Fcgr3* in these aberrant neutrophils were significantly reduced, which indicated their immature characteristics (Figure S4C). A recent single cell sequencing data clarified the heterogeneity of neutrophil development and identified 8 (G0-G5c) developing neutrophil subpopulations by 24 marker genes (Xie et al., 2020). From this, the expression of the 24 marker genes in aberrant neutrophils were also analyzed. The results showed that, compared with the normal neutrophils in control group, only the expression of G1 maker genes were significantly increase in these aberrant neutrophils (Figure 3E). This suggested that these abnormal neutrophils were similar to the G1 developing neutrophils. In addition, the RNA-seq data of lungs in mice infected by

SARS-CoV-2 and IAV also showed that the G5b mature neutrophils were primarily activated in IAV infection, while most neutrophils recruited in SARS-CoV-2 infection is G1 to G4 subpopulation (Figure S4D and S4E). Together, these suggested that coronavirus infection induced a population of dysplastic aberrant neutrophils, and may cause the dysregulation of the innate immune system.

Paquinimod suppresses the accumulation of aberrant neutrophils and coronavirus infection

Aberrant neutrophils coiled around the emergence of symptoms in mice, suggesting that they may be responsible for the fatal infection of coronavirus. Additionally, as the main cytoplasmic protein of neutrophils, S100A8 has great influence on the function of neutrophils. Therefore, to further clarify the role of S100A8 in the emergence of the aberrant neutrophils and coronavirus infection, we designed experiments to suppress the effects of S100A8/A9. Paquinimod can prevent the binding of S100A9 to TLR-4 (Bjork et al., 2009; Schelbergen et al., 2015), suggesting that it can be used to block the function of S100A8/A9. Thus, we treated the mice intranasally with Paquinimod after SARS-CoV-2 and MHV infection (Figure 4A). Excitingly, the treatment of Paquinimod successfully improved the living state of mice (Figure 4B). Histopathological and immunohistochemical staining of the lungs showed that both the pulmonary interstitium damage and the invasion of neutrophils ($S100A8^{+}$) were alleviated via Paquinimod treatment (Figure 4C and 4D). Further detection found that *S100a8* and *Ly6g* expression and viral loads including SARS-CoV-2 and MHV in the mice that were successfully rescued by Paquinimod were significantly reduced (Figure 4E, 4F, S5A and S5B). Subsequently, neutrophils in Paquinimod-treated mice were analyzed by flow cytometry. As expected, compared with the coronavirus infection group, most neutrophils in Paquinimod-treated mice returned to normal $CD45^{+}CD11b^{+}Ly6G^{high}$ (Figure 4G and S5C). These results indicated that Paquinimod successfully rescued mice from fatal outcome from coronavirus infection. However，Paquinimod did not

succeed in rescuing IAV-infected mice that did not show high *S100a8* expression and aberrant neutrophils (Figure 2C and S5D). Paquinimod likely blocked the function of S100A8/A9 specifically, thereby preventing the accumulation of aberrant neutrophils and fatal coronavirus infection.

To evaluate the effect of Paquinimod on the modulation of immune responses in coronavirus infected mice, the RNA-seq analysis of lungs was performed. In the case of MHV infection, neutrophil chemotaxis and anti-bacterial responses were significantly downregulated after Paquinimod treatment (Figure S5E). The expression of neutrophil marker genes was also reduced by Paquinimod (Figure S5F). Meanwhile, as an important component of the adaptive immune system that plays a major antiviral role, B cells signaling pathway are significantly activated after Paquinimod treatment (Figure 4E and S5G). Further qRT-PCR analysis showed that, consistent with MHV infection, the B cell marker gene *Cd19* in SARS-CoV-2 infection was also gradually restored and showed a tendency of up-regulation after Paquinimod treatment (Figure 4H, 4I and S5H). These suggested that Paquinimod treatment contributed to the recovery of the aberrant immune response caused by the coronavirus, which in turn promotes the elimination of the virus.

S100A8/A9 mediates the emergence of aberrant neutrophils in a TLR4 dependent manner

Paquinimod treatment, which is able to inhibit the function of S100A8/A9 by blocking the binding of S100A9 to TLR4, suppressed the accumulation of aberrant neutrophils and rescued mice from fatal coronavirus infection. This suggested that the TLR4 signaling pathway may play an important role in coronavirus-induced fatal infections. To make this clear, we treated mice infected by coronavirus including SARS-CoV-2 and MHV with TLR4 signaling inhibitor. Resatorvid is a selective TLR4 inhibitor, which can down-regulate expression of TLR4 downstream signaling molecules. Through Resatorvid treatment, we found that the proportion of aberrant neutrophils in

coronavirus-infected mice were significantly reduced (Figure 5A and 5B). Consistently, Resatorvid also inhibited *S100a8* and *Ly6g* expression and viral replication in lungs of the infected mice (Figure 5C and 5D). Besides, it is believed that S100A8/A9 can also activate the receptor for advanced glycation end products (RAGE) pathways (Narumi et al., 2015). To this end, we also treated mice infected by SARS-CoV-2 and MHV with RAGE inhibitor (Azeliragon). The results showed that Azeliragon treatment did not significantly prevent the production of aberrant neutrophils and viral replication (Figure S6A and S6B). This implied the critical role of the TLR4 signaling pathway in coronavirus infection. A previous study showed that S100A8/A9 can promote granulopoiesis by activating macrophages and common myeloid progenitor (Nagareddy et al., 2013). Thus, to further confirm the role of TLR4 in activating S100A8 related signaling, we treated wild type or MyD88 deficient mouse macrophages Raw264.7 with the recombinant S100A8/A9. MyD88 is an important adaptor protein, and the absence of MyD88 can lead to the suppression of TLR4 signaling (Figure S6C). The detection results showed that recombinant S100A8/A9 was able to induce the expression of *S100a8* and neutrophil chemokine *Cxcl2* in a TLR4/MyD88 dependent manner (Figure 5E). This reflected that S100A8 was able to induce the expression of itself, thereby forming a positive loop and amplifying the aberrant responses.

Discussion

The endogenous danger-associated molecular patterns (DAMPs) are able to trigger the activation of innate immune signaling. Alarmins are a panel of proteins or peptides that can function as DAMPs to activate various immune pathways (Bianchi, 2007; Yang et al., 2017). The fine tuning of alarmins expression is critical for maintaining immune homoeostasis. Over or sustained expression of alarmins can result in uncontrolled inflammation and cytokine storm (Chan et al., 2012; Cher et al., 2018; Kang et al., 2014; Patel, 2018). Here, we demonstrated that coronavirus, SARS-CoV-2 and MHV, induced

a robust transcription of the alarmin S100A8, which in turn led to innate antiviral immune disorder. These results were consistent with the recent studies which revealed that S100A8/A9 (calprotectin) was highly elevated in patients with COVID-19, and a prognosticator of negative outcomes (Shi et al., 2020; Silvin et al., 2020). In addition to S100A8, several alarmins had also been found to be up-regulated in COVID-19 patients, which may be influenced by multiple factors, such as the course of the disease, treatment drugs and so on. Therefore, their role in COVID-19 patients still needs to be further explored. During SARS-CoV-2 infection, the induction of type I IFNs is inhibited and neutrophils abnormally response, and similar phenotypes were observed during MHV infection. The type I IFNs are the primary antiviral effectors that are usually induced at the very early stage of viral infection. Thus, the inhibition of type I IFNs suggests a disruption of the classical antiviral immune response. Meanwhile, a good deal of literatures has shown that the induction of type I IFNs was also suppressed during SARS-CoV infection (Channappanavar et al., 2016; Chu et al., 2020; Frieman et al., 2010; Matsuyama et al., 2020; Zornetzer et al., 2010). These studies suggested that delayed type I IFNs induction was responsible for lethal pneumonia in SARS-COV-infected mice. Therefore, exploring the mechanism of type I IFNs suppression may be of great significance for the containment of coronavirus infection.

IFNAR deficient mice have been suggested as a potential animal model for SARS-CoV-2 experiments (Hanifehnezhad et al., 2020). In this study, we attempted to establish a mouse model of coronavirus-related severe acute respiratory distress syndrome (ARDS) by MHV. The results showed that in IFNAR deficient mice, MHV successfully invaded the lung of the mice and induced an immune response similar to SARS-CoV-2 infection. This suggested that it seems like a shared mechanism that directs the pathogenesis of pneumonia during SARS-CoV-2 infection and MHV infection. Thus, IFNAR deficient mice infected by MHV may serve as useful models for investigating ARDS associated with SARS-CoV-2 infection. Besides, the susceptibility of IFNAR deficient mice to coronavirus suggested that type I IFNs

signaling pathway may be important for resistance to coronavirus infection. IRF3 and IRF7 are key transcription factors of type I IFNs (Honda et al., 2006; You et al., 2013). However, IRF3/IRF7 double knockout mice challenged with MHV did not develop obvious ARDS. Additionally, both previous studies and our data showed that induction of type I IFNs is blocked during SARS-CoV-2 and MHV infections (Hadjadj et al., 2020; Zhou et al., 2020). These suggested that IFNAR may exert an unknown mechanism during resistance to coronavirus infection in a type I IFNs independent way.

Neutrophil abnormalities were defined during SARS-CoV-2 infection through our study. Neutrophils are usually activated during bacterial infection to kill invading bacteria (Deng et al., 2013; Li et al., 2002). However, in COVID-19 patients with severe symptoms, neutrophils were found to be significantly increased (Kuri-Cervantes et al., 2020; Liao et al., 2020; Tan et al., 2020; Wu et al., 2020a). It was originally thought that the increase in neutrophils in severe COVID-19 patients may be attributed to co-infection of bacteria. However, several reports, including our study, have found that the increase of neutrophils was not due to bacterial co-infection but to a group of aberrant neutrophils induced by SARS-CoV-2 infection. Further, both our study and recent studies had identified that these abnormal neutrophils showed obvious immature characteristics (Schulte-Schrepping et al., 2020; Silvin et al., 2020; Wilk et al., 2020). This is consistent with the basic characteristics of myeloid-derived suppressor cells (MDSCs). The presence of G-MDSCs may explain reduced white blood cell levels in severe COVID-19 patients. Besides, the current study also found that thrombosis in COVID-19 was associated with higher levels of circulating neutrophil extracellular traps (NETs) and calprotectin (S100A8/A9) (Shi et al., 2020; Zuo et al., 2020). The formation of NETs is one of the main ways in which neutrophils function (Ali et al., 2019; Meng et al., 2017; Yadav et al., 2019). Therefore, it is worthwhile to investigate if these aberrant neutrophils cause the increase and dysfunction of circulating NETs. In short, the exact function of these aberrant neutrophils and the mechanism of aberrant neutrophils induced by coronavirus infection remains to be further explored.

406 Our study showed the importance of the TLR4 signaling pathway in the formation of
407 fatal infections by coronavirus. Through blocking TLR4 signaling, both Paquinimod
408 and Resatorvid improved the health status of coronavirus infected mice. Previous
409 SARS-CoV studies also showed that TLRs, including TLR3, TLR4, TLR7 and TLR8,
410 mediated antiviral responses (Li et al., 2016; Li et al., 2013; Totura et al., 2015).
411 Meanwhile, *Tlr3*$^{-/-}$ and *Tlr4*$^{-/-}$ mice also showed greater susceptibility to SARS-CoV
412 than wild-type mice and the deficiency of TLRs adaptor proteins TRIF or MyD88
413 resulted in higher mortality of mice during SARS-CoV infection (Totura et al., 2015).
414 All these suggested that TLRs signaling also plays an important role in SARS-CoV
415 infection, which further reflects the close relationship between TLRs signals and
416 coronavirus infection. However, it was unknown how TLR4 signaling was activated by
417 coronavirus infection. We here found that the sharp up-regulation of S100A8 in
418 coronavirus infection may be responsible for activation of TLR4 signaling. S100A8 is
419 the main cytoplasmic protein of mature neutrophils. Thus, during the initial phase of
420 SARS-CoV-2 infection, *S100a8* was slightly induced in lungs at 1dpi, possibly due to
421 the recruitment of mature neutrophils into the lungs (Figure 2C). The RNA-seq data
422 also showed that the marker gene *Cxcr2* of mature neutrophils was up-regulated at 1 dpi
423 during SARS-CoV-2 infection. Thus, it is possible that mature neutrophils that invaded
424 the lungs carried large amounts of S100A8/A9, which can further induce the expression
425 of itself. This may from a positive loop to amplify the aberrant response. Excessive and
426 uncontrolled S100A8/A9 production strongly stimulates the TLR4 signal, which
427 induces the aberrant neutrophils and imbalance of immune response. However, the
428 exact mechanism of S100A8 surge and TLR4 signal activation induced by coronavirus
429 infection remains to be further explored. A recent study predicted that antigenic
430 epitopes within the full-length S-protein of SARS-CoV-2 may bind to TLR4/MD-2
431 complex and activate immune response (Bhattacharya et al., 2020). Based on this, there
432 might be a possibility that SARS-CoV-2 could directly stimulate the expression of
433 S100A8/A9 by TLR4 signaling. As SARS-CoV-2 is an RNA virus, it is also reasonable

that SARS-CoV-2 could induce neutrophilic S100A8/A9 expression by activating RNA sensing pathways, such as RIG-I-like receptor, TLR3 and TLR7/8 signaling. Moreover, TLR4 of macrophages can also be activated by S100A8/A9. Although the expression level of S100A8 is low, the function of it in Raw 274.7 cells has been validated previously (Muller et al., 2017). We here also observed the induction of *S100a8* and *Cxcl2* by the treatment of S100A8/A9 (Figure 5E). Besides, the induction of proinflammatory cytokines, such as IL-1B and IL-6, in macrophages or the bronchoalveolar lavage fluid (BALF) by S100A8/A9 is also noteworthy. However, these views still need to be supported by more data in the future.

In summary, we have demonstrated that coronavirus infection including SARS-CoV-2 and MHV leads to the disorder of antiviral innate immunity. It has been shown that alarmin S100A8 was robustly up-regulated and a group of aberrant premature neutrophils were induced. TLR4 signaling may mediate this abnormal immune response. The inhibitors of S100A8/A9-TLR4 axis were able to mitigate the abnormality of antiviral immunity and inhibit viral replication. These results uncover the characteristic of innate immunity in the pathogenesis of SASR-CoV-2 infection and provide therapeutic targets for the treatment of COVID-19.

Limitations of the study

In the rhesus macaque infection model, neutrophil abnormalities were only indirectly reflected by RNA-seq data and were not visualized by cell staining due to the limitations of the associated antibodies. Although we have shown that Paquinimod and Resatorvid are effective in preventing SARS-CoV-2 infection, their efficacy in rescuing rhesus macaques infected with SARS-CoV-2 was not further tested due to limited experimental conditions. The absence of severe disease in SARS-CoV-2-infected hACE2 mice largely limited the progress of the study, which may be due to the limited replication of the virus in hACE2 mice. This also makes that the data on weight loss of mice may seem unconvincing. Although we supplemented experimental data on mouse

coronavirus MHV infection similar to SARS-CoV-2 infection, the consistency of the two coronavirus infection mechanisms cannot be fully assured. The presence of abnormal immature neutrophils may be an important cause of severe disease during SARS-CoV-2 infection. In experiments, we found that these abnormal immature neutrophils were likely MDSCs, which effectively inhibited the production and activation of other immune cells and led to immune system disorders. This may be the root cause of the virus replication outbreak, and the detailed process needs to be further explored. SARS-CoV-2 infection was effectively inhibited by targeting S100A8/A9-TLR4 axis inhibition. However, it is still unknown how SARS-CoV-2 infection induces the elevated expression of S100A8/A9 in the first place. Furthermore, the drug regimens of Paquinimod and Resatorvid need to be further optimized. In experiments, we found that poor drug use regimens had the opposite effect for reasons that are still unknown. We have developed a relatively effective drug regimen in mice, but the optimal drug regimen needs to be further explored. Collectively, the study contains many limitations, but the innate immune abnormalities and possible drug targets proposed in this study provide new therapy ideas for COVID-19.

Acknowledgments

This work was supported by the National Natural Science Foundation of China (31570891; 31872736; 32022028), the National Key Research and Development Program of China (2016YFA0500302; 2020YFA0707800), the National Key Research and Development Program (2020YFA0707500) and the Strategic Priority Research Program (XDB29010000), Peking University Clinical + X（PKU2020LCXQ009). Xiangxi Wang was supported by Ten Thousand Talent Program and the NSFS Innovative Research Group (81921005). We thank National Mega projects of China for Major Infectious Diseases (2017ZX10304402), CAMS initiative for Innovative Medicine of China (2016-12M-2-006) and The National Natural Science Foundation of China (Grant No. 82041008 and 32070543）for the support on the animal model

development and experiments.

Author Contributions

F.Y., X.W., C.Q. and Q.G. conceived the study and analyzed the data. Q.G., Y.Z., J.Li., J.Liu. and Y.X. performed most experiments and analyzed the data. F.Y. and X.G. analyzed the RNA-seq data. M.K. and N.W. helped with the in vitro cell experiments. H.X. helped with the flow cytometry experiments. L.B., D.W., H.Z. and R.G. helped with the rhesus macaques and *hACE2* mice related experiments. Z.Z., L.C., Y.L. and S.L. helped with the other mice experiments. Y.L., X.W, X. Wei, L. Chen and J. Chen provided support on literature search. F.Y. wrote the paper. F.Y., X.W. and C.Q. revised the paper.

Declaration of Interests

The authors have no conflicts of interest to declare.

Figure legends

Figure 1. *S100A8* and neutrophil-related genes expression were significantly induced in the early stage of SARS-CoV-2 infection.

(A) A flow chart depicting the process of animal experiments with rhesus macaques. Rhesus macaques (3-4 years old) were challenged with 10^6 TCID50 SARS-CoV-2 virus by intratracheal routes.

(B) Go analysis of the differences in rhesus macaques infected with SARS-CoV-2 compared with Mock (*Fold Change (FC) > 4 or < 0.25, P value < 0.05*).

(C) Analysis of neutrophil marker genes expression. *n = 4*.

(D) Volcano plots show differentially expressed genes in rhesus macaques infected with SARS-CoV-2 at 3 dpi and 5 dpi. *S100A8* expression is significantly increased after SARS-CoV-2 infection.

(E) Analysis of all known alarmins showing that *S100A8* is the most significantly induced one.

(F) qRT-PCR analysis for viral loads and the expression of *S100A8* and *S100A9* in the lungs of SARS-CoV-2-infected rhesus macaques at 3 dpi and 5 dpi. *n = 3*.

(G) Heat map shows alarmins in the blood from rhesus macaques infected with SARS-CoV-2 at 5dpi (left). The expression of neutrophil marker genes was analyzed (FC to mock, right). *n = 4*.

(H) Heat map depicting the expression of alarmins of the lung samples from healthy control and post-mortem lung samples from COVID-19 patients (left). The expression of neutrophil marker genes analyzed (FC to healthy control, right). Data from the lungs of COVID-19 patients and healthy control correspond to GEO: GSE147507.

(**P < 0.05; **P < 0.01; ***P < 0.001*).

Figure 2. Antiviral innate immune disorder and aberrant *S100a8* expression induced by coronavirus but no other viruses.

(A) A flow chart depicting the process of animal experiments with mice. All the mice

were inoculated intranasally with viruses. Virus dose: SARS-CoV-2 (10^5 TCID50), IAV (10^5 TCID50), EMCV (10^7 PFU), HSV-1 (10^6 PFU), MHV-A59 (10^5 PFU).

(B) RNA-seq analysis of lungs from mice infected with SARS-CoV-2 or IAV. Go analysis was performed with the differentially expressed genes compared with Mock (*FC > 4 or < 0.25, P value < 0.05*). *n = 3.*

(C) qRT-PCR analysis for the expression of *S100a8, Ly6g, Ifnb* and *Isg15* in the lungs of mice at different time points after IAV or SARS-CoV-2 infection. *n = 3*.

(D) Heat map depicting the expression differences of neutrophil marker genes in the lungs of mice infected with IAV or SARS-CoV-2.

(E) qRT-PCR analysis for the expression of *S100a8* and *Ly6g* in the blood and lungs of mice infected with different viruses. *n = 3*.

(F) Post-infection survival curves of wild type mice and *Ifnar*$^{-/-}$ mice infected with MHV. *n = 10*.

(G) RNA-seq analysis of the lungs of *Ifnar*$^{-/-}$ mice infected with MHV at 5 dpi. Go and KEGG analysis were performed with the differentially expressed genes compared with Mock (*FC > 4 or < 0.25, P value < 0.05*).

(H) qRT-PCR analysis for the expression of *Ifnb, Isg15, S100a8* and *Ly6g* in the lungs of *Ifnar*$^{-/-}$ mice infected with IAV or MHV at 5 dpi. *n = 3*.

(**P < 0.05; **P < 0.01; ***P < 0.001*).

Figure 3. A group of immature aberrant neutrophils emerged in coronavirus-infected mice.

(A) Immunohistochemical analysis of the location and expression of S100A8 in the lung tissue of mice infected with SARS-CoV-2 or MHV at 5 dpi. The S100A8$^+$ cells in the lungs of mice infected with coronavirus were increased significantly. The red arrows indicate the S100A8$^+$ cells. *n = 5.*

(B) Flow cytometry analysis of neutrophils in lungs from mice infected with SARS-CoV-2 and MHV at 5 dpi. Control group means mice treated with Vehicle. Gate

P1 shows the conventional neutrophils ($CD45^+CD11b^+Ly6G^{high}$), and Gate P2 shows the pathologic aberrant neutrophils ($CD45^+CD11b^+Ly6G^{variable}$). Aberrant neutrophils (P2) in the lungs of mice infected with coronavirus were significantly increased. *n = 3.*

(C) Flow cytometry analysis of neutrophils in lungs of mice challenged with IAV, EMCV, HSV-1 and LPS at 5 dpi. The results showed that these treatments did not induce an increase in aberrant neutrophils. *n = 3.*

(D) Flow cytometry analysis of neutrophils in bone marrow from mice infected with SARS-CoV-2 and MHV at 5 dpi. *n = 3.*

(E) qRT-PCR analyzed related genes expression of aberrant neutrophils in bone marrow of mice infected with MHV at 5 dpi and identified the differentiated types of aberrant neutrophils. *n = 3.*

(****P < 0.001*).

Figure 4. Paquinimod rescues the mice infected by SARS-CoV-2 and MHV.

(A) A flow chart depicting the process of a drug rescue experiment.

(B) Analysis of weight and survival rate of mice infected with SARS-CoV-2 and MHV after Paquinimod treatment. *n=6.*

(C) Analysis of the rescue effect of Paquinimod by H&E staining and pathology score of lung tissue in mice infected with SARS-CoV-2 or MHV at 5 dpi. Paquinimod treatment significantly prevented the bleeding and fibrosis in lung tissue. A number of pulmonary H&E staining images were randomly selected for pathological scoring. *n = 10.*

(D) Immunohistochemical analysis of the $S100A8^+$ cells in the lung tissue of mice infected with SARS-CoV-2 or MHV at 5 dpi after Paquinimod treatment. The $S100A8^+$ cells in the lungs of mice infected with coronavirus were decreased significantly after Paquinimod treatment. The red arrows indicate the $S100A8^+$ cells. *n = 5.*

(E) qRT-PCR analysis for the expression of *S100a8* and *Ly6g* in the lung of mice infected with SARS-CoV2 at 5 dpi after Paquinimod treatment. *n = 3.*

(F) qRT-PCR analysis of viral loads in the lungs of mice infected with coronavirus SARS-CoV-2 and MHV at 5 dpi after Paquinimod treatment. *n = 3.*

(G) Flow cytometry analysis of neutrophils in lungs, blood and bone marrow from mice infected with SARS-CoV-2 at 5 dpi after Paquinimod treatment. $CD45^{+}CD11b^{+}Ly6G^{variable}$ aberrant neutrophils (P2) in the mice infected with SARS-CoV-2 were significantly decreased by Paquinimod treatment. *n = 3.*

(H) Heat map depicting a decrease in B cell related gene expression in the lungs of mice infected with SARS-CoV-2.

(I) qRT-PCR analysis for the expression of B cell marker gene *Cd19* in the peripheral blood of mice infected with SARS-CoV2 after Paquinimod treatment. $n \geq 5$.

(**P < 0.05; **P < 0.01; ***P < 0.001*).

Figure 5. Blocking TLR4 signal can alleviate coronavirus fatal infection.

(A)-(B) Flow cytometry analysis of neutrophils in lungs, blood and bone marrow from mice infected with SARS-CoV-2 (A) and MHV (B) at 5 dpi after Resatorvid treatment. Aberrant neutrophils (P2) in the mice infected with coronavirus were significantly decreased by Resatorvid treatment. *n = 3.*

(C)-(D) qRT-PCR analysis for the expression of *S100a8, Ly6g* and viral loads in the lungs of mice infected with SARS-CoV-2 (C) and MHV (D) at 5 dpi after Resatorvid treatment. *n = 3.*

(E) qRT-PCR analysis for the effect of recombinant S100A8/A9 on *S100a8* and *Cxcl2* expression through TLR4 pathway. *n = 3.*

(**P < 0.05; **P < 0.01; ***P < 0.001*).

STAR Methods

RESOURCE AVAILABILITY

Lead Contact

Further information and requests for resources and reagents should be directed to and

will be fulfilled by the Lead Contact, Fuping You (fupingyou@hsc.pku.edu.cn).

Materials Availability

This study did not generate new unique reagents.

Data and Code Availability

The datasets generated during this study are available at Gene Expression Omnibus (https://www.ncbi.nlm.nih.gov/geo/). The original data of the RNA-seq were uploaded to the Gene Expression Omnibus (GEO) DataSets (GEO: GSE158297).

EXPERIMENTAL MODEL AND SUBJECT DETAILS

Cells

Raw 274.7 cells, 17CL-1 cells, A549 cells and Vero cells were kept in our lab. Raw 274.7 cells and A549 cells were cultured in RPMI 1640 medium (Gibco) supplemented with 10% FBS, 100 U/mL Penicillin-Streptomycin. 17CL-1 cells and Vero cells were cultured in DMEM medium (Gibco) supplemented with 10% FBS (PAN), 100 U/mL Penicillin-Streptomycin. All cells were incubated at 37 °C, 5% CO2.

Viruses

A stock of the SARS-CoV-2 virus (WH-09/human/2020/CHN, accession No. MT093631.2) was used in this study. IAV (Influenza a Virus, PR8) was a gift from Feng Qiang (Fudan University) and HSV-1 (Herpes simplex virus 1) was from A. Iwasaki (Yale University). EMCV (Encephalomyocarditis virus, VR-129B) was purchased from American Type Culture Collection (ATCC). MHV-A59 (mouse hepatitis virus A-59) has been described previously and was kept in our lab (Yang et al., 2014).

Seed SARS-CoV-2 stocks and virus isolation studies were performed in Vero E6 cells, and the virus titer were determined using a standard TCID50 assay.

IAV was propagated in 10-day-old specific-pathogen-free embryonic chicken eggs. The allantoic fluid was collected and titrated to determine the TCID50 in A549 cells.

EMCV, HSV-1 were propagated in Vero cells, and the supernatants were used as a stock solution. The titer of viruses was determined by plaque assay in Vero cells.

MHV-A59 were propagated in 17CL-1 cells, and the supernatants were used as a stock solution. The titer of the virus was determined by plaque assay in 17CL-1 cells.

Animal experiments

All experiments with live SARS-CoV-2 viruses were carried out in the enhanced biosafety level 3 (P3+) facilities in the Institute of Laboratory Animal Science, Chinese Academy of Medical Sciences (CAMS) approved by the National Health Commission of the People's Republic of China. All animals care and use were in accordance with the Guide for the Care and Use of Laboratory Animals of the Chinese Association for Laboratory Animal Science. All procedures of animal handling were approved by the Animal Care Committee of Peking University Health Science Center.

All animals were kept and bred in specific pathogen-free conditions under controlled temperature (23 ± 1 °C) and exposed to a constant 12 h light-dark cycle. All animals are guaranteed adequate clean water and nutritious feed. Rhesus macaques used in this study were provided by the Institute of Laboratory Animal Science, Chinese Academy of Medical Science. Wild-type (WT) C57BL/6 mice were purchased from Department of Laboratory Animal Science of Peking University Health Science Center, Beijing. The *hACE2* transgenic mice, which were generated by microinjection of the mouse Ace2 promoter driving the human ACE2 coding sequence into the pronuclei of fertilized ova from ICR mice (Bao et al., 2020), were obtained from the Institute of Laboratory Animal Science, Peking Union Medical College. Interferon-α receptor gene knockout (*Ifnar*$^{-/-}$) mice is a gift from Pro. Erol Fikrig (Yale University). *Irf3/7* double knockout mice is a gift from Pro. Zhengfan Jiang (Peking University). Before the experimental operation, all animals are test or drug naïve without involvement in any previous procedures. They are healthy and have normal immunity.

METHOD DETAILS

Animal Infection assays

For animal infection assay, rhesus macaques (3-4 years old) were anaesthetized with 10 mg/kg ketamine hydrochloride and challenged with 10^6 TCID50 SARS-CoV-2 virus by intratracheal routes. The hACE2 mice were intraperitoneally anaesthetized by 2.5% avertin with 0.02 mL/g body weight and inoculated intranasally with SARS-CoV-2 virus at a dosage of 10^5 TCID50. WT C57BL/6J mice and *Ifnar*$^{-/-}$ mice were anaesthetized by isoflurane. All the mice used were adults aged 6-12 weeks. Age-matched mice were used in the same experiment. IAV is inoculated intranasally at a dosage of 10^5 TCID50. The doses of other inoculated viruses: EMCV (10^7 PFU), HSV-1 (10^6 PFU), MHV-A59 (10^5 PFU). The animals intranasally inoculated with an equal volume of PBS were used as a mock control. The health status and weight of all mice were observed and recorded daily. Rhesus macaques were euthanized at 0, 3- and 5-days post infection (dpi) to collect different tissues and examined virus replication and histopathological changes. Mice were euthanized at 0, 1, 3, 5 and 7 dpi to collect different tissues and examined virus replication and histopathological changes. All the mice depicted in the study are female. However, through observation, we found that male mice seem to die more quickly than female mice after MHV-A59 infection, which may be related to hormonal metabolism between males and females.

RNA sequencing (RNA-seq)

Whole RNA of tissues with specific treatment were purified using TRNzol reagent. The transcriptome library for sequencing was generated using VAHTSTM mRNA-seq v2 Library Prep Kit for Illumina® (Vazyme Biotech Co.,Ltd, Nanjing, China) following the manufacturer's recommendations. After clustering, the libraries were sequenced on Illumina Hiseq X Ten platform using (2×150 bp) paired-end module. The raw data were transformed into raw reads by base calling using CASAVA.

Quantitative RT-PCR (qRT-PCR) analysis

Total RNA was isolated from the tissues by TRNzol reagent (DP424, Beijing TIANGEN Biotech, China). Then, cDNA was prepared using HiScript III 1st Strand cDNA Synthesis Kit (R312-02, Nanjing Vazyme Biotech, China). qRT-PCR was performed using the Applied Biosystems 7500 Real-Time PCR Systems (Thermo Fisher Scientific, USA) with SYBR qPCR Master mix (Q331-02, Nanjing Vazyme Biotech, China). The data of qRT-PCR were analyzed by the Livak method ($2^{-\Delta\Delta Ct}$). Ribosomal protein L19 (RPL19) was used as a reference gene for mice, and GAPDH for macaques. The *E* gene of SARS-CoV-2, *N* gene of MHV-A59 and *M1* gene of IAV are examined for quantitation. All gene primers are displayed in supplementary materials Table S1.

Histology and Immunohistochemical staining

The lungs were quickly placed in cold saline solution and rinsed after they were collected. Then, lungs were fixed in 4% paraformaldehyde, dehydrated and embedded in paraffin prior to sectioning at 5 μm, and sections were stained with hematoxylin and eosin. Several pulmonary H&E staining images were randomly selected for pathological scoring in a blinded fashion. Lung damage is classified into five levels by pathological scoring. "0" represents no abnormality, "1" represents very small pathological changes, "2" represents slight pathological changes, "3" represents moderate pathological changes and "4" represents serious pathological changes.

For immunohistochemical staining, the lung paraffin sections were dewaxed and rehydrated through xylene and an alcohol gradient. Antigen retrieval was performed by heating the sections to 100 °C for 4 min in 0.01 M citrate buffer (pH 6.0) and repeated 4 times. The operations were performed according to the instructions of the two-step detection kit (PV-9001, Beijing ZSGB Biotechnology, China). The samples were treated by endogenous peroxidase blockers for 10 min at room temperature followed by incubation with primary antibodies S100A8 (1:200, 47310T, Cell Signaling Technology) at 37°C for 1 h, then after washed with PBS. The samples were incubated with reaction enhancer for 20 min at room temperature and secondary

antibodies at 37°C for 30 min, and finally sections were visualized by 3,30-diaminobenzidine tetrahydrochloride (DAB) and counterstained with haematoxylin.

Tissue preparation and flow cytometry

The lung tissues, peripheral blood and bone marrow were collected from the mice. The lungs were first ground with 200-mesh copper sieve, and then transferred to DMEM containing 10% FBS, 0.5 mg/mL Collagenase D (11088858001, Roche, Switzerland) and 0.1 mg/mL DNase I (07469, STEMCELL Technologies, Canada) for a 20 min digestion at 37□ to obtain single-cell suspensions. Bone marrow were flushed out of the femurs using a 23–gauge needle in PBS containing 2mM EDTA and 2% fetal bovine serum (FBS) and dispersed into single cells through a pipette. Single-cell samples were treated by red blood cell lysis buffer (R1010, Beijing Solarbio Science & Technology, China) for 2 min at room temperature and passed through a 200-mesh copper sieve before staining. Peripheral blood was treated with red blood cell lysis buffer to remove red blood cells.

After blocking non-specific Fc receptor-mediated interactions with CD16/CD32 antibodies (14-0161-82, eBioscience, USA), single-cell suspensions were stained with fluorophore-conjugated anti-mouse antibodies at 4□ for 30min. After washing the samples, flow cytometry acquisition was performed on a BD LSRFortessa. Sorting were performed using a BD AriaIII (BD). All antibodies were purchased from eBioscience: CD45-PE (12-0451-81), Ly-6G-APC (17-9668-80), and CD11b-FITC (11-0112-81).

Drug rescue assay

For the Paquinimod rescue assay, all mice were challenged by viruses and randomly divided into two groups, in which one group was given intranasally 12.5 μg/day of Paquinimod (TargetMol; Catalog No. T7310) starting on 2 dpi and the other group was treated with equal volume PBS as the control group. Stock solutions of 100 mg/mL Paquinimod were prepared with DMSO in advance. The health status and

weight of all mice were observed and recorded daily.

For the Resatorvid/Azeliragon rescue assay, the mice challenged by viruses were given intraperitoneally 50 μg/day of Resatorvid (MCE; Synonyms: TAK-242; CLI-095) and 100 μg/day of Azeliragon (TargetMol; Catalog No. T2507) starting on 2 dpi. Stock solutions of 10 mM Resatorvid and 10 mM Azeliragon were prepared with DMSO in advance and was diluted by corn oil. The control group mice were given intraperitoneally 200 μL of corn oil solution which contained 20 μL of DMSO. The health status and body weight of all mice were observed and recorded daily.

Cell co-culture assay

Raw 264.7 cells were seeded on 6-well plates with 10^6 cells/mL. After cell adherence, LPS (100 ng/mL) and mS100A8/A9 protein (1 μM) with or without Resatorvid (100 nM) were added. After 12 hours co-culture, cells were harvested and lysed by TRNzol reagent for RNA extraction. Then, the expression of related genes was detected by qRT-PCR.

QUANTIFICATION AND STATISTICAL ANALYSIS

RNA-seq analysis

The FastQC and Trim Galore were used for raw data quality control, then the R package Rsubread was used for mapping and counting the reads. The count matrix was normalized by FPKM. The differentially expressed genes were identified by the GFOLD, a Linux software. The GO and KEGG annotations of DEGs were performed in the DAVID database (https://david.ncifcrf.gov/home.jsp).

Data analysis for flow cytometry data

Flow cytometry data analysis was performed with FlowJo V10.0.7. Relative cell percentage was used for visualization.

Statistical analysis

All analyses were repeated at least three times, and a representative experimental result was presented. Prism 8 software (Graphic software) was used for survival

785 curves, charts and statistical analyses. Two-tailed unpaired Student's t test was used
786 for statistical analysis to determine significant differences when a pair of conditions
787 was compared. Asterisks denote statistical significance (*$P < 0.05$; **$P < 0.01$; ***
788 $P < 0.001$). The data are reported as the mean ± S.D. The exact value of n representing
789 number of animals are included in each figure legend.
790

791 ## Supplemental item

792 **Table S1. Sequences of qRT-PCR primers. Related to STAR Methods.**
793

794 ## References

795 Akira, S., Uematsu, S., and Takeuchi, O. (2006). Pathogen recognition and innate
796 immunity. Cell *124*, 783-801.
797 Ali, R.A., Gandhi, A.A., Meng, H., Yalavarthi, S., Vreede, A.P., Estes, S.K., Palmer,
798 O.R., Bockenstedt, P.L., Pinsky, D.J., Greve, J.M., *et al.* (2019). Adenosine receptor
799 agonism protects against NETosis and thrombosis in antiphospholipid syndrome. Nat
800 Commun *10*, 1916.
801 Bao, L., Deng, W., Huang, B., Gao, H., Liu, J., Ren, L., Wei, Q., Yu, P., Xu, Y., Qi, F.,
802 et al. (2020). The pathogenicity of SARS-CoV-2 in hACE2 transgenic mice. Nature
803 *583*, 830-833.
804 Bhattacharya, M., Sharma, A.R., Mallick, B., Sharma, G., Lee, S.S., and Chakraborty,
805 C. (2020). Immunoinformatics approach to understand molecular interaction between
806 multi-epitopic regions of SARS-CoV-2 spike-protein with TLR4/MD-2 complex.
807 Infect Genet Evol, 104587.
808 Bianchi, M.E. (2007). DAMPs, PAMPs and alarmins: all we need to know about
809 danger. J Leukoc Biol *81*, 1-5.
810 Bjork, P., Bjork, A., Vogl, T., Stenstrom, M., Liberg, D., Olsson, A., Roth, J., Ivars, F.,
811 and Leanderson, T. (2009). Identification of human S100A9 as a novel target for
812 treatment of autoimmune disease via binding to quinoline-3-carboxamides. PLoS Biol

7, e97.

Blanco-Melo, D., Nilsson-Payant, B.E., Liu, W.C., Uhl, S., Hoagland, D., Moller, R., Jordan, T.X., Oishi, K., Panis, M., Sachs, D., *et al.* (2020). Imbalanced Host Response to SARS-CoV-2 Drives Development of COVID-19. Cell *181*, 1036-1045 e1039.

Chakraborty, D., Zenker, S., Rossaint, J., Holscher, A., Pohlen, M., Zarbock, A., Roth, J., and Vogl, T. (2017). Alarmin S100A8 Activates Alveolar Epithelial Cells in the Context of Acute Lung Injury in a TLR4-Dependent Manner. Front Immunol *8*, 1493.

Chan, J.K., Roth, J., Oppenheim, J.J., Tracey, K.J., Vogl, T., Feldmann, M., Horwood, N., and Nanchahal, J. (2012). Alarmins: awaiting a clinical response. J Clin Invest *122*, 2711-2719.

Channappanavar, R., Fehr, A.R., Vijay, R., Mack, M., Zhao, J., Meyerholz, D.K., and Perlman, S. (2016). Dysregulated Type I Interferon and Inflammatory Monocyte-Macrophage Responses Cause Lethal Pneumonia in SARS-CoV-Infected Mice. Cell Host Microbe *19*, 181-193.

Chen, G.Y., and Nunez, G. (2010). Sterile inflammation: sensing and reacting to damage. Nat Rev Immunol *10*, 826-837.

Cher, J.Z.B., Akbar, M., Kitson, S., Crowe, L.A.N., Garcia-Melchor, E., Hannah, S.C., McLean, M., Fazzi, U.G., Kerr, S.C., Murrell, G.A.C., *et al.* (2018). Alarmins in Frozen Shoulder: A Molecular Association Between Inflammation and Pain. Am J Sports Med *46*, 671-678.

Chu, H., Chan, J.F., Wang, Y., Yuen, T.T., Chai, Y., Hou, Y., Shuai, H., Yang, D., Hu, B., Huang, X., *et al.* (2020). Comparative Replication and Immune Activation Profiles of SARS-CoV-2 and SARS-CoV in Human Lungs: An Ex Vivo Study With Implications for the Pathogenesis of COVID-19. Clin Infect Dis *71*, 1400-1409.

Deng, Q., Sarris, M., Bennin, D.A., Green, J.M., Herbomel, P., and Huttenlocher, A. (2013). Localized bacterial infection induces systemic activation of neutrophils through Cxcr2 signaling in zebrafish. J Leukoc Biol *93*, 761-769.

Diao, B., Wang, C., Tan, Y., Chen, X., Liu, Y., Ning, L., Chen, L., Li, M., Liu, Y.,

Wang, G., *et al.* (2020). Reduction and Functional Exhaustion of T Cells in Patients With Coronavirus Disease 2019 (COVID-19). Front Immunol *11*, 827.

Feng, J., Meyer, C.A., Wang, Q., Liu, J.S., Shirley Liu, X., and Zhang, Y. (2012). GFOLD: a generalized fold change for ranking differentially expressed genes from RNA-seq data. Bioinformatics *28*, 2782-2788.

Frieman, M.B., Chen, J., Morrison, T.E., Whitmore, A., Funkhouser, W., Ward, J.M., Lamirande, E.W., Roberts, A., Heise, M., Subbarao, K., *et al.* (2010). SARS-CoV pathogenesis is regulated by a STAT1 dependent but a type I, II and III interferon receptor independent mechanism. PLoS Pathog *6*, e1000849.

Foell, D., Frosch, M., Sorg, C., and Roth, J. (2004). Phagocyte-specific calcium-binding S100 proteins as clinical laboratory markers of inflammation. Clin Chim Acta *344*, 37-51.

Giri, K., Pabelick, C.M., Mukherjee, P., and Prakash, Y.S. (2016). Hepatoma derived growth factor (HDGF) dynamics in ovarian cancer cells. Apoptosis *21*, 329-339.

Hadjadj, J., Yatim, N., Barnabei, L., Corneau, A., Boussier, J., Smith, N., Pere, H., Charbit, B., Bondet, V., Chenevier-Gobeaux, C., *et al.* (2020). Impaired type I interferon activity and inflammatory responses in severe COVID-19 patients. Science *369*, 718-724.

Hanifehnezhad, A., Kehribar, E.S., Oztop, S., Sheraz, A., Kasirga, S., Ergunay, K., Onder, S., Yilmaz, E., Engin, D., Oguzoglu, T.C., *et al.* (2020). Characterization of local SARS-CoV-2 isolates and pathogenicity in IFNAR(-/-) mice. Heliyon *6*, e05116.

Huang, C., Wang, Y., Li, X., Ren, L., Zhao, J., Hu, Y., Zhang, L., Fan, G., Xu, J., Gu, X., *et al.* (2020). Clinical features of patients infected with 2019 novel coronavirus in Wuhan, China. The Lancet *395*, 497-506.

Kang, R., Chen, R., Zhang, Q., Hou, W., Wu, S., Cao, L., Huang, J., Yu, Y., Fan, X.G., Yan, Z., *et al.* (2014). HMGB1 in health and disease. Mol Aspects Med *40*, 1-116.

Kuri-Cervantes, L., Pampena, M.B., Meng, W., Rosenfeld, A.M., Ittner, C.A.G., Weisman, A.R., Agyekum, R.S., Mathew, D., Baxter, A.E., Vella, L.A., *et al.* (2020).

869 Comprehensive mapping of immune perturbations associated with severe COVID-19.
870 Sci Immunol *5*.
871 Li, Y., Chen, M., Cao, H., Zhu, Y., Zheng, J., and Zhou, H. (2013). Extraordinary
872 GU-rich single-strand RNA identified from SARS coronavirus contributes an
873 excessive innate immune response. Microbes Infect *15*, 88-95.
874 Li, Y.M., Karlin, A., Loike, J.D., and Silverstein, S.C. (2002). A critical concentration
875 of neutrophils is required for effective bacterial killing in suspension. P Natl Acad Sci
876 USA *99*, 8289-8294.
877 Li, S.W., Wang, C.Y., Jou, Y.J., Huang, S.H., Hsiao, L.H., Wan, L., Lin, Y.J., Kung,
878 S.H., and Lin, C.W. (2016). SARS Coronavirus Papain-Like Protease Inhibits the
879 TLR7 Signaling Pathway through Removing Lys63-Linked Polyubiquitination of
880 TRAF3 and TRAF6. Int J Mol Sci *17*.
881 Liao, M., Liu, Y., Yuan, J., Wen, Y., Xu, G., Zhao, J., Cheng, L., Li, J., Wang, X.,
882 Wang, F., *et al.* (2020). Single-cell landscape of bronchoalveolar immune cells in
883 patients with COVID-19. Nat Med *26*, 842-844.
884 Liao, Y., Smyth, G.K., and Shi, W. (2019). The R package Rsubread is easier, faster,
885 cheaper and better for alignment and quantification of RNA sequencing reads. Nucleic
886 Acids Res *47*, e47.
887 Matsuyama, T., Kubli, S.P., Yoshinaga, S.K., Pfeffer, K., and Mak, T.W. (2020). An
888 aberrant STAT pathway is central to COVID-19. Cell Death Differ. https://doi.org/
889 10.1038/s41418-020-00633-7
890 Meng, H., Yalavarthi, S., Kanthi, Y., Mazza, L.F., Elfline, M.A., Luke, C.E., Pinsky,
891 D.J., Henke, P.K., and Knight, J.S. (2017). In Vivo Role of Neutrophil Extracellular
892 Traps in Antiphospholipid Antibody-Mediated Venous Thrombosis. Arthritis
893 Rheumatol *69*, 655-667.
894 Muller, I., Vogl, T., Pappritz, K., Miteva, K., Savvatis, K., Rohde, D., Most, P.,
895 Lassner, D., Pieske, B., Kuhl, U., *et al.* (2017). Pathogenic Role of the
896 Damage-Associated Molecular Patterns S100A8 and S100A9 in Coxsackievirus

B3-Induced Myocarditis. Circ-Heart Fail *10*.

Nathan, C. (2002). Points of control in inflammation. Nature *420*, 846-852.

Nagareddy, P.R., Murphy, A.J., Stirzaker, R.A., Hu, Y., Yu, S., Miller, R.G., Ramkhelawon, B., Distel, E., Westerterp, M., Huang, L.S., *et al.* (2013). Hyperglycemia promotes myelopoiesis and impairs the resolution of atherosclerosis. Cell Metab *17*, 695-708.

Narumi, K., Miyakawa, R., Ueda, R., Hashimoto, H., Yamamoto, Y., Yoshida, T., and Aoki, K. (2015). Proinflammatory Proteins S100A8/S100A9 Activate NK Cells via Interaction with RAGE. J Immunol *194*, 5539-5548.

Nauseef, W.M., and Borregaard, N. (2014). Neutrophils at work. Nat Immunol *15*, 602-611.

Nicolas-Avila, J.A., Adrover, J.M., and Hidalgo, A. (2017). Neutrophils in Homeostasis, Immunity, and Cancer. Immunity *46*, 15-28.

Ometto, F., Friso, L., Astorri, D., Botsios, C., Raffeiner, B., Punzi, L., and Doria, A. (2017). Calprotectin in rheumatic diseases. Exp Biol Med (Maywood) *242*, 859-873.

Oppenheim, J.J., and Yang, D. (2005). Alarmins: chemotactic activators of immune responses. Curr Opin Immunol *17*, 359-365.

Patel, S. (2018). Danger-Associated Molecular Patterns (DAMPs): the Derivatives and Triggers of Inflammation. Curr Allergy Asthma Rep *18*, 63.

Schelbergen, R.F., Geven, E.J., van den Bosch, M.H., Eriksson, H., Leanderson, T., Vogl, T., Roth, J., van de Loo, F.A., Koenders, M.I., van der Kraan, P.M., *et al.* (2015). Prophylactic treatment with S100A9 inhibitor paquinimod reduces pathology in experimental collagenase-induced osteoarthritis. Ann Rheum Dis *74*, 2254-2258.

Schulte-Schrepping, J., Reusch, N., Paclik, D., Bassler, K., Schlickeiser, S., Zhang, B., Kramer, B., Krammer, T., Brumhard, S., Bonaguro, L., *et al.* (2020). Severe COVID-19 Is Marked by a Dysregulated Myeloid Cell Compartment. Cell *182*, 1419-1440 e1423.

Shi, H., Zuo, Y., Yalavarthi, S., Gockman, K., Zuo, M., Madison, J.A., Blair, C.,

Woodward, W., Lezak, S.P., Lugogo, N.L., *et al.* (2020). Neutrophil calprotectin identifies severe pulmonary disease in COVID-19. J Leukoc Biol. https://doi.org/10.1002/JLB.3COVCRA0720-359R

Silvin, A., Chapuis, N., Dunsmore, G., Goubet, A.G., Dubuisson, A., Derosa, L., Almire, C., Henon, C., Kosmider, O., Droin, N., *et al.* (2020). Elevated Calprotectin and Abnormal Myeloid Cell Subsets Discriminate Severe from Mild COVID-19. Cell *182*, 1401-1418 e1418.

Tan, L., Wang, Q., Zhang, D., Ding, J., Huang, Q., Tang, Y.Q., Wang, Q., and Miao, H. (2020). Lymphopenia predicts disease severity of COVID-19: a descriptive and predictive study. Signal Transduct Target Ther *5*, 33.

Totura, A.L., Whitmore, A., Agnihothram, S., Schafer, A., Katze, M.G., Heise, M.T., and Baric, R.S. (2015). Toll-Like Receptor 3 Signaling via TRIF Contributes to a Protective Innate Immune Response to Severe Acute Respiratory Syndrome Coronavirus Infection. mBio *6*, e00638-00615.

Vogl, T., Tenbrock, K., Ludwig, S., Leukert, N., Ehrhardt, C., van Zoelen, M.A., Nacken, W., Foell, D., van der Poll, T., Sorg, C., *et al.* (2007). Mrp8 and Mrp14 are endogenous activators of Toll-like receptor 4, promoting lethal, endotoxin-induced shock. Nat Med *13*, 1042-1049.

Wang, H., Liao, H., Ochani, M., Justiniani, M., Lin, X., Yang, L., Al-Abed, Y., Wang, H., Metz, C., Miller, E.J., *et al.* (2004). Cholinergic agonists inhibit HMGB1 release and improve survival in experimental sepsis. Nat Med *10*, 1216-1221.

Wang, S., Song, R., Wang, Z., Jing, Z., Wang, S., and Ma, J. (2018). S100A8/A9 in Inflammation. Front Immunol *9*, 1298.

Wilk, A.J., Rustagi, A., Zhao, N.Q., Roque, J., Martinez-Colon, G.J., McKechnie, J.L., Ivison, G.T., Ranganath, T., Vergara, R., Hollis, T., *et al.* (2020). A single-cell atlas of the peripheral immune response in patients with severe COVID-19. Nat Med *26*, 1070-1076.

Wu, C., Chen, X., Cai, Y., Xia, J., Zhou, X., Xu, S., Huang, H., Zhang, L., Zhou, X.,

Du, C., *et al.* (2020a). Risk Factors Associated With Acute Respiratory Distress Syndrome and Death in Patients With Coronavirus Disease 2019 Pneumonia in Wuhan, China. JAMA Intern Med. https://doi.org/10.1001/jamainternmed.2020.0994

Wu, F., Zhao, S., Yu, B., Chen, Y.M., Wang, W., Song, Z.G., Hu, Y., Tao, Z.W., Tian, J.H., Pei, Y.Y., *et al.* (2020b). A new coronavirus associated with human respiratory disease in China. Nature *579*, 265-269.

Xie, X., Shi, Q., Wu, P., Zhang, X., Kambara, H., Su, J., Yu, H., Park, S.Y., Guo, R., Ren, Q., *et al.* (2020). Single-cell transcriptome profiling reveals neutrophil heterogeneity in homeostasis and infection. Nat Immunol. https://doi.org/10.1038/s41590-020-0736-z

Yadav, V., Chi, L., Zhao, R., Tourdot, B.E., Yalavarthi, S., Jacobs, B.N., Banka, A., Liao, H., Koonse, S., Anyanwu, A.C., *et al.* (2019). Ectonucleotidase tri(di)phosphohydrolase-1 (ENTPD-1) disrupts inflammasome/interleukin 1beta-driven venous thrombosis. J Clin Invest *129*, 2872-2877.

Yang, Han, Z., and Oppenheim, J.J. (2017). Alarmins and immunity. Immunol Rev *280*, 41-56.

Yang, Z., Du, J., Chen, G., Zhao, J., Yang, X., Su, L., Cheng, G., and Tang, H. (2014). Coronavirus MHV-A59 infects the lung and causes severe pneumonia in C57BL/6 mice. Virologica Sinica *29*, 393-402.

You, F., Wang, P., Yang, L., Yang, G., Zhao, Y.O., Qian, F., Walker, W., Sutton, R., Montgomery, R., Lin, R., *et al.* (2013). ELF4 is critical for induction of type I interferon and the host antiviral response. Nat Immunol *14*, 1237-1246.

Zhang, B., Zhou, X., Qiu, Y., Song, Y., Feng, F., Feng, J., Song, Q., Jia, Q., and Wang, J. (2020). Clinical characteristics of 82 cases of death from COVID-19. PLoS One *15*, e0235458.

Zheng, H.Y., Zhang, M., Yang, C.X., Zhang, N., Wang, X.C., Yang, X.P., Dong, X.Q., and Zheng, Y.T. (2020a). Elevated exhaustion levels and reduced functional diversity of T cells in peripheral blood may predict severe progression in COVID-19 patients.

Cell Mol Immunol *17*, 541-543.

Zheng, M., Gao, Y., Wang, G., Song, G., Liu, S., Sun, D., Xu, Y., and Tian, Z. (2020b). Functional exhaustion of antiviral lymphocytes in COVID-19 patients. Cell Mol Immunol *17*, 533-535.

Zhou, P., Liu, Z., Chen, Y., Xiao, Y., Huang, X., and Fan, X.G. (2020). Bacterial and fungal infections in COVID-19 patients: A matter of concern. Infect Control Hosp Epidemiol, 1-2.

Zhu, N., Zhang, D., Wang, W., Li, X., Yang, B., Song, J., Zhao, X., Huang, B., Shi, W., Lu, R., *et al.* (2020). A Novel Coronavirus from Patients with Pneumonia in China, 2019. N Engl J Med *382*, 727-733.

Zornetzer, G.A., Frieman, M.B., Rosenzweig, E., Korth, M.J., Page, C., Baric, R.S., and Katze, M.G. (2010). Transcriptomic analysis reveals a mechanism for a prefibrotic phenotype in STAT1 knockout mice during severe acute respiratory syndrome coronavirus infection. J Virol *84*, 11297-11309.

Zuo, Y., Yalavarthi, S., Shi, H., Gockman, K., Zuo, M., Madison, J.A., Blair, C., Weber, A., Barnes, B.J., Egeblad, M., *et al.* (2020). Neutrophil extracellular traps in COVID-19. JCI Insight *5*.

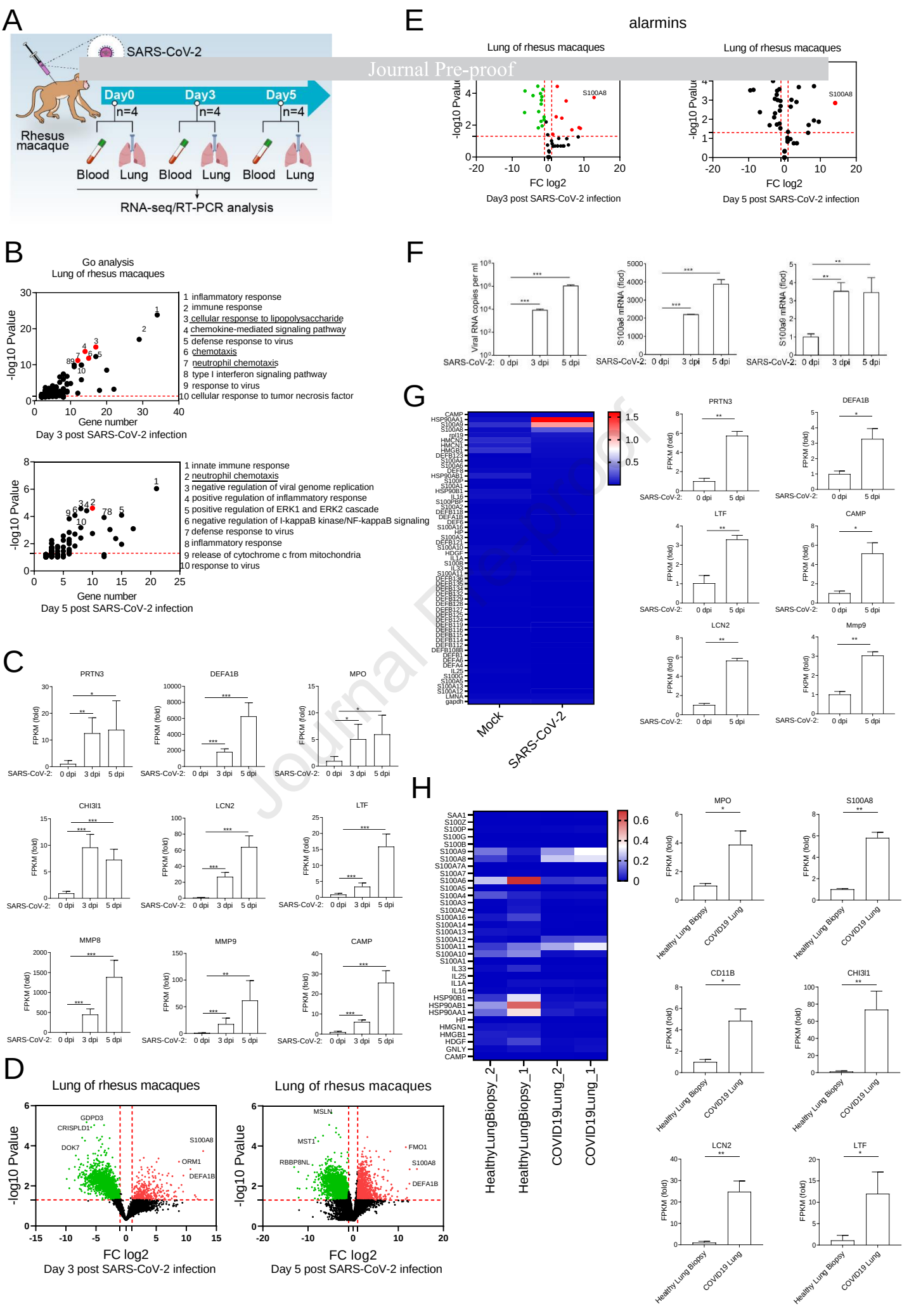

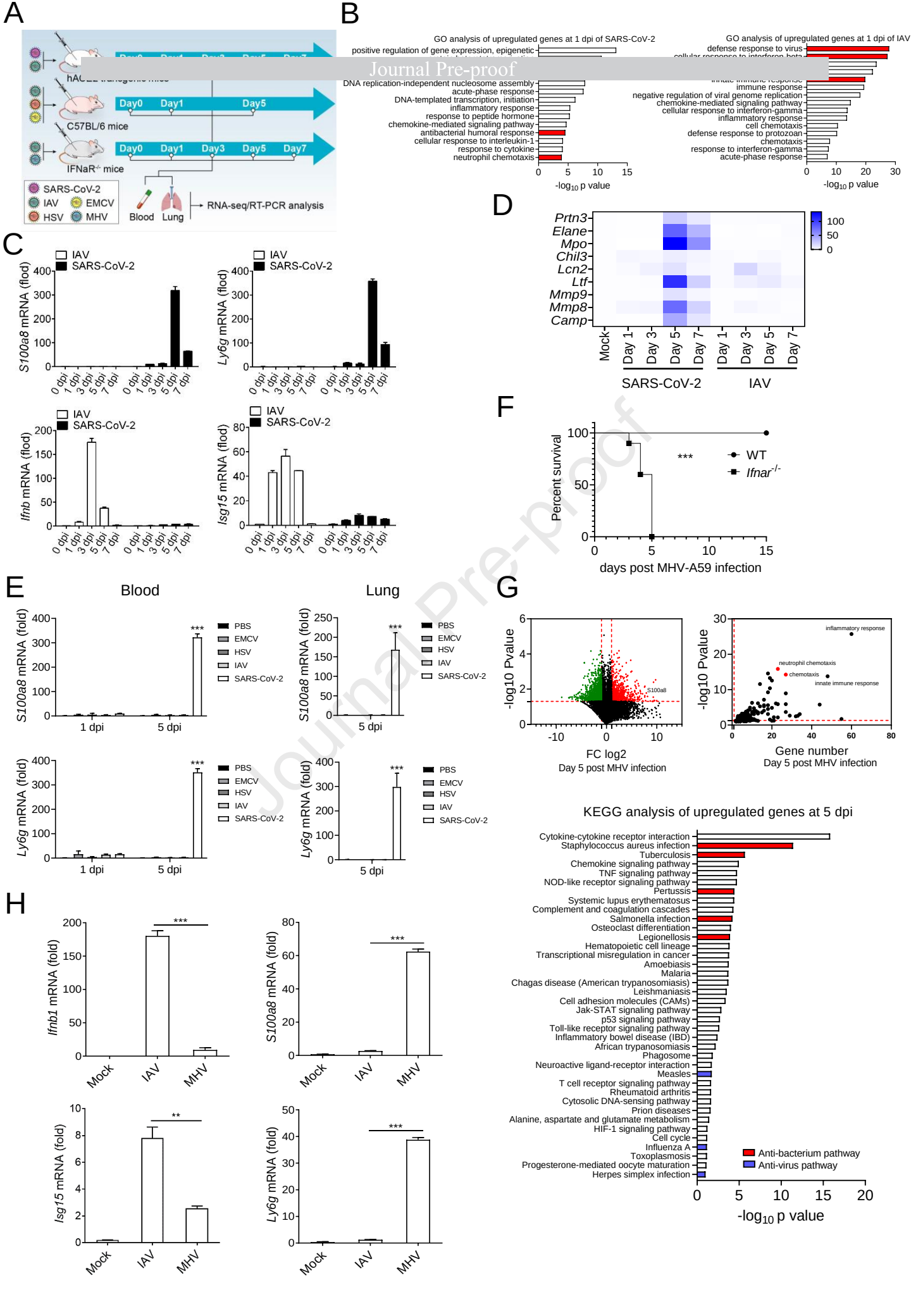

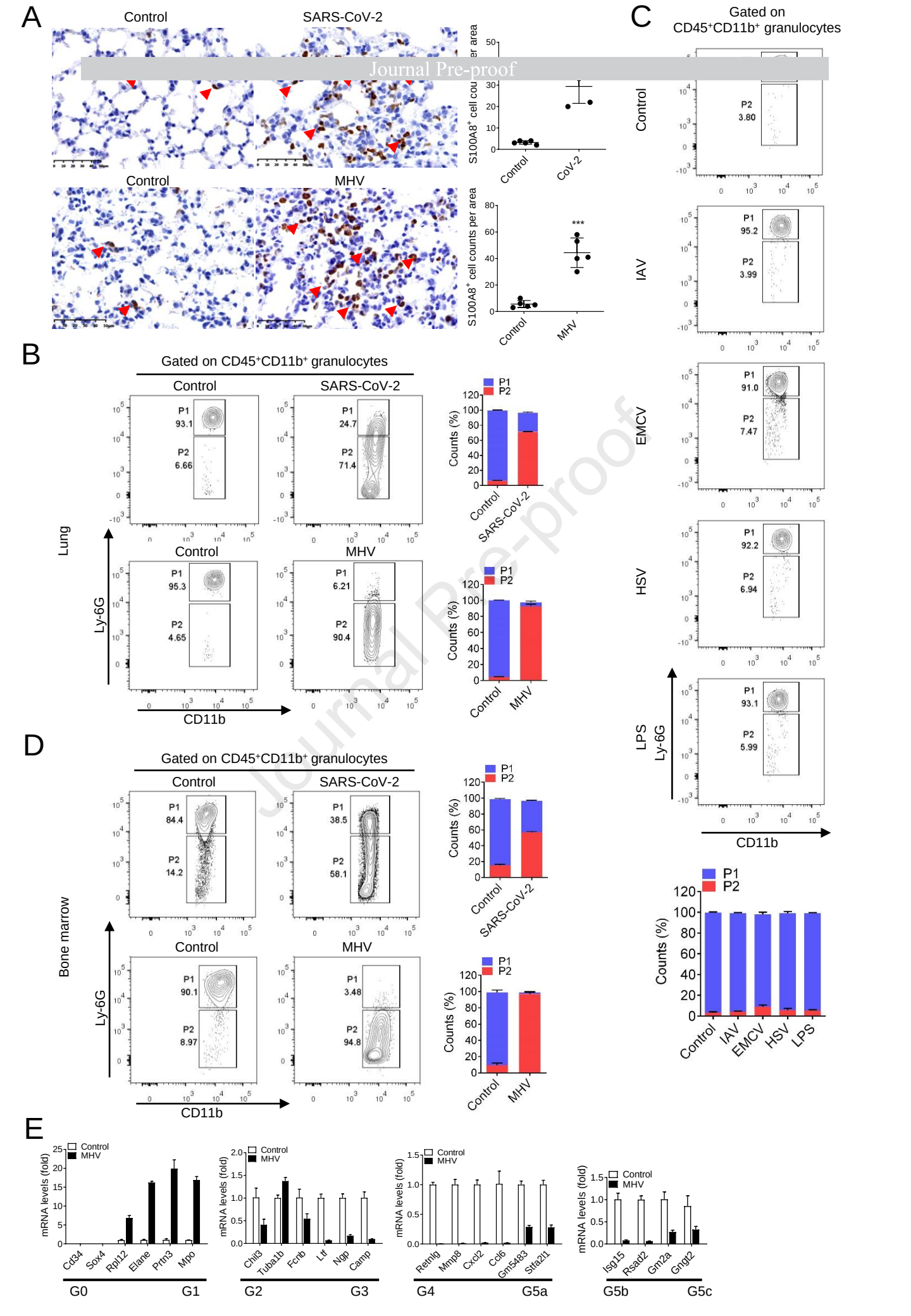

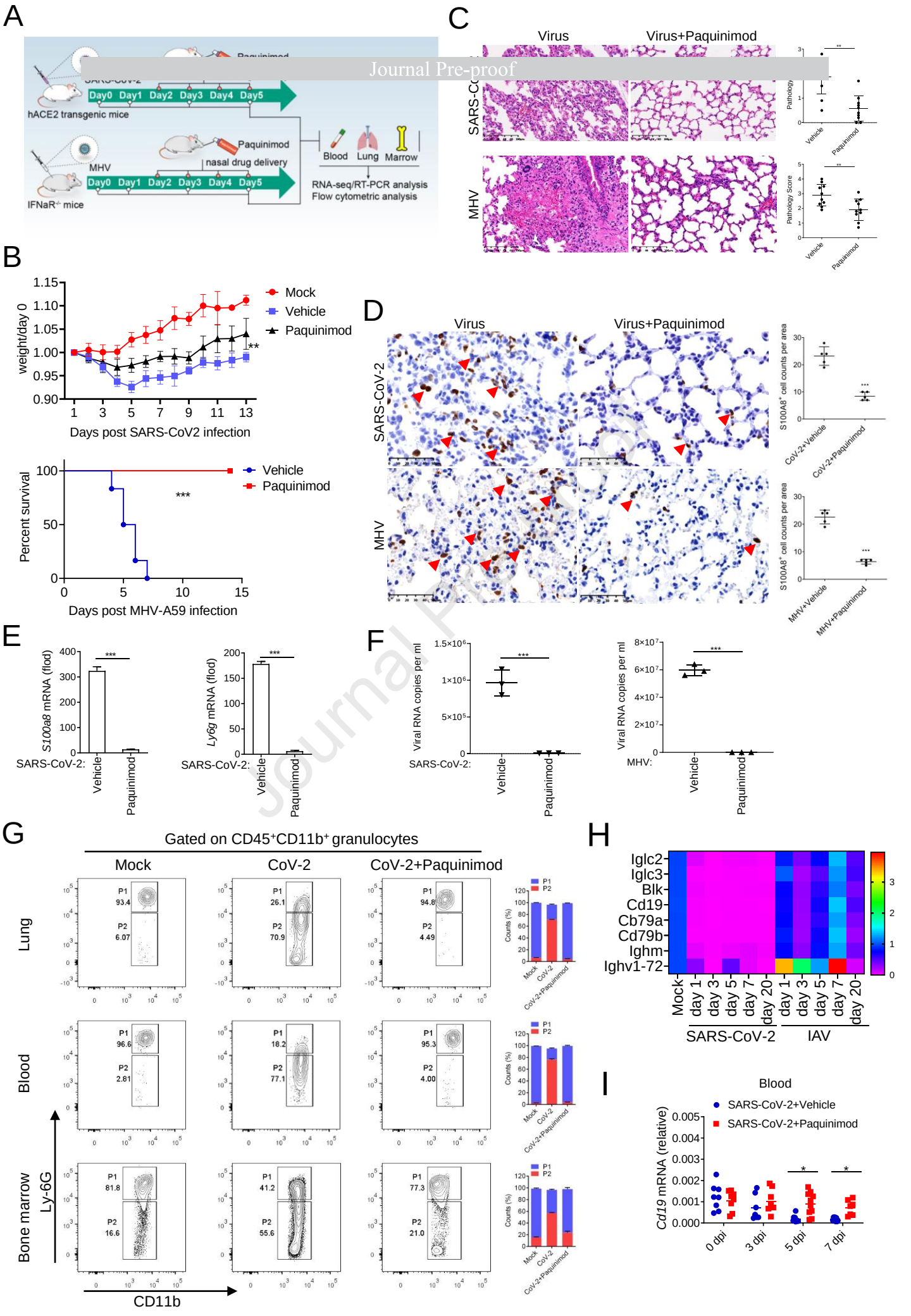

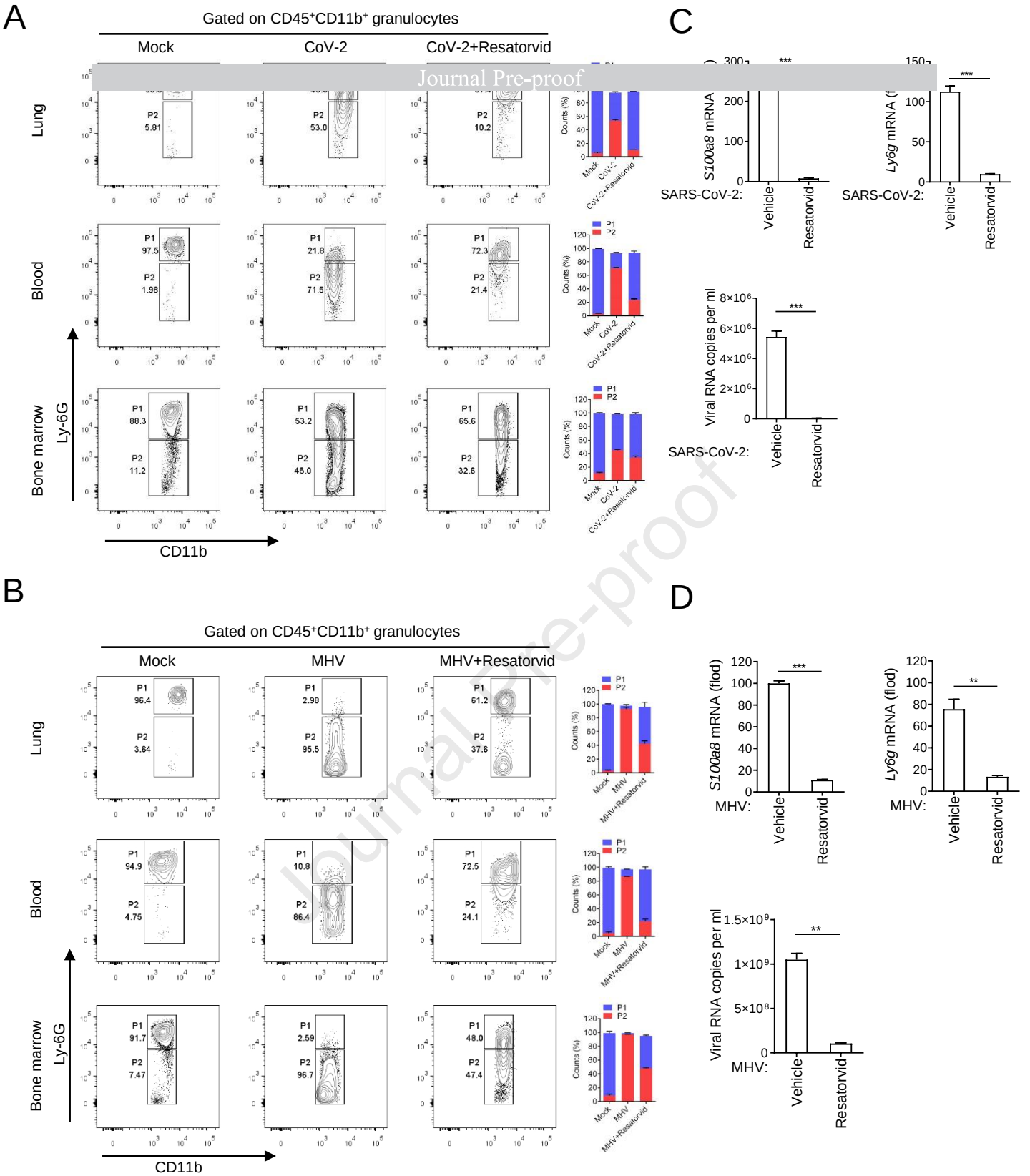

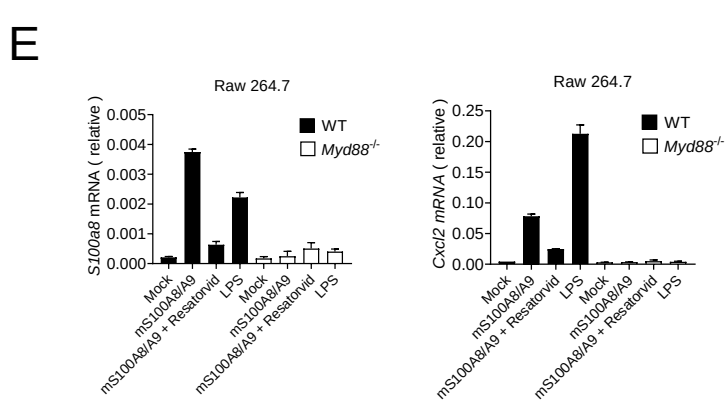

Highlights

- S100A8 is dramatically up-regulated in SARS-CoV-2 infected animal models and patients.
- A group of aberrant immature neutrophils is induced during SARS-CoV-2 infection.
- Immune disorder is mediated by the S100A8/A9-TLR4 pathway.
- S100A8/A9 inhibitor, Paquinimod, could prevent COVID-19 associated immune disorder.

eTOC blurb

Authors

Qirui Guo, Yingchi Zhao, Junhong Li, …, Chuan Qin, Xiangxi Wang, Fuping You

Correspondence

qinchuan@pumc.edu.cn (C.Q.), xiangxi@ibp.ac.cn (X.-X.W.),

fupingyou@hsc.pku.edu.cn (F.-P.Y.)

In brief

Guo et al. demonstrate that over activation of S100A8/A9-TLR4 signaling results in immune imbalance and expansion of aberrant immature neutrophils during SARS-CoV-2 infection. Relevant therapeutic targets were validated in animal infection models.